ELSEVIER

Polymer 42 (2001) 9995–10006

polymer

www.elsevier.com/locate/polymer

Macromolecule–metal complexes: ligand field stabilization and thermophysical property modification

Laurence A. Belfiore*, Mary Pat McCurdie, Pronab K. Das

Polymer Physics and Engineering Laboratory, Department of Chemical Engineering, Colorado State University, Fort Collins, CO 80523, USA

Received 19 March 2001; received in revised form 5 June 2001; accepted 7 June 2001

Abstract

When transition metal cations coordinate to ligands in the sidegroup of a polymer and modify the thermal response of a macromolecular complex, the enhancement in T_g can be explained by focusing on ligand field stabilization of the metal d-electrons. The methodology to identify attractive coordination complexes and predict relative increases in T_g is described in terms of the local symmetry of the complex, the molecular orbital pattern, and the d-electron configuration. Interelectronic repulsion is considered for pseudo-octahedral d^6 and d^7 complexes in the glassy state when there is ambiguity in the order in which the d-orbitals are populated. Ligand field stabilization energies are calculated for simple octahedral geometries, as well as 5-coordinate complexes with reduced symmetry, such as square pyramidal, trigonal bipyramidal, and pentagonal planar. If the transition metal cation bridges two different macromolecules in the glassy state via coordination crosslinks, then 5-coordinate complexes with one surviving metal–polymer bond above T_g represent reasonable geometries in the molten state. This model of thermochemical synergy in macromolecule–metal complexes with no adjustable parameters considers the glass transition as an endothermic process in which sufficient thermal energy must be supplied to dissociate intermolecular bridges or coordination crosslinks and produce coordinatively unsaturated molten state complexes. The enhancement in T_g correlates well with the difference between ligand field stabilization energies in the glassy and molten states for $Ru^{2+}(d^6)$, $Co^{2+}(d^7)$, and $Ni^{2+}(d^8)$ complexes with either poly(4-vinylpyridine), or poly(L-histidine). Larger increases in T_g are measured in complexes with the synthetic poly(α-amino acid) relative to those with poly(4-vinylpyridine), but the universality of the model is not sufficient to predict relative T_g enhancements in complexes with different polymers.

Keywords: Glass transition temperature enhancement; Transition metal coordination complexes; Ligand exchange

1. Introduction

1.1. Polymeric coordination complexes with d-block salts

Unlike the well-known phenomenon of plasticization [1], transition metal salts typically increase the glass transition temperature of polymers which contain attractive ligands in the sidegroup [2]. The mechanism involves acid–base interactions between the metal center and appropriate functional groups in the polymer via ligand exchange [3]. Whereas plasticizers interact weakly with the polymer via van der Waals forces and enhance the fractional free volume of the binary mixture [4,5], metal–ligand σ-bonds form between transition metals and favorable functional groups in the macromolecule [6]. Since coordination numbers between four and six are quite common in d-block complexes [7], opportunities exist for basic ligands in the sidegroup of the polymer to occupy sites in the 1st -shell coordination sphere of an acidic metal center. The concept of coordination crosslinks is realized when functional groups from more than one chain occupy sites in the 1st-shell of a single metal center [8]. This type of structure exhibits reduced mobility in the vicinity of these thermoreversible crosslinks, which is consistent with an increase in T_g. Multifunctional metal centers which coordinate to basic ligands in several different chains [9] could be responsible for the formation of nanoclusters with significant reduction in chain mobility and dramatic increases in T_g. This has been observed recently in polymeric complexes with several lanthanide trichloride hydrates from lanthanum to lutetium in the 1st-row of the f-block [10,11]. In addition to increasing T_g, macromolecule–metal complexes could form gels during preparation in dilute solution [10,12,13]. When gelation occurs in aqueous media [10], applications for water purification, controlled release and artificial muscles become attractive [14]. If gels exhibit pH and temperature sensitivity, then it might be possible to exploit these 'molecular gates'

* Corresponding author. Tel.: +1-970-491-5395; fax: +1-970-491-7369.
E-mail address: belfiore@engr.colostate.edu (L.A. Belfiore).

0032-3861/01/$ - see front matter
PII: S0032-3861(01)00459-1

and use them for controlled release of encapsulated molecules with a specific target. Of particular interest in this research contribution, the methodology for producing macromolecule–metal complexes with significantly enhanced glass transition temperatures is discussed from an energetic viewpoint which considers the stabilization of metal d-electrons [8,15]. A systematic study of T_g enhancement in poly(4-vinylpyridine) and poly(L-histidine) via ruthenium(II), cobalt(II) and nickel(II) is employed to illustrate the methodology. Both polymers contain nitrogen lone pairs in either the pyridine sidegroup or the imidazole ring of the histidine sidegroup which form σ-bonds with the appropriate d-orbitals of the transition metal cation. It should be emphasized that most of these T_g data have been published before [2,8,9,15–17]. However, Ru^{2+} complexes with poly(L-histidine) have only been discussed in the PhD thesis of M.P. McCurdie [18]. The primary objective of this contribution was to describe transition-metal-induced enhancements of T_g in selected amorphous polymers via ligand field stabilization energy differences between complexes in the glassy and molten states. The ligand field model considers a reduction in symmetry and a decrease in coordination number of the metal center above T_g due to dissociation of a ligand in the polymer's sidegroup from the 1st-shell coordination sphere. Geometric distortions of 3-coordinate and 5-coordinate polymer–metal complexes in the molten state are also considered.

1.2. Ruthenium d^6 complexes

Ruthenium(II) is attractive because strong-field low-spin d^6 metal centers with pseudo-octahedral symmetry exhibit very large ligand field splittings and stabilization energies [6], as discussed below. Ru^{2+} is classified as a borderline acid [19,20] which exhibits an affinity for borderline bases, like pyridine ligands in the sidegroup of poly(4-vinylpyridine). Reactions of a particular ruthenium dimer [i.e. $\{Ru(CO)_3Cl_2\}_2$] with both stoichiometric and excess amounts of pyridine are well documented [21–23]. In both cases, the dihalogen bridge is cleaved and either one or two pyridine ligands coordinate to each metal center forming complexes with pseudo-octahedral symmetry. The 1st pyridine ligand occupies the vacant site generated from cleavage of the bridge, and the 2nd pyridine ligand displaces carbon monoxide in the coordination sphere of the metal [23]. Vibrational spectroscopic studies of $[Ru(CO)_3Cl_2]_2$ in the vicinity of 1900–2200 cm^{-1} fingerprint the infrared absorptions of CO which are sensitive to σ-donation and π back-donation [23–25]. Electron-rich metal centers backbond to π-acceptor ligands like CO and shift the vibrational absorption frequencies of carbon monoxide to lower energy [6]. Solid state carbon-13 NMR spectroscopic data reveal that heteronuclear spin diffusion between protons in poly(4-vinylpyridine) and the carbonyl carbons of $[Ru(CO)_3Cl_2]_2$ is operative [2,15]. This observation of intermolecular polarization transfer is consistent with micromixing and/or complexation of two dissimilar components.

1.3. Cobalt d^7 complexes

Cobalt chloride hexahydrate was used to generate transition metal complexes with amino, pyridine and imidazole ligands in the sidegroup of poly(vinylamine), poly(4-vinylpyridine) and poly(L-histidine), respectively. Two independent x-ray crystallographic studies [26,27] have deduced a pseudo-octahedral geometry for $CoCl_2(H_2O)_6$ with two chloride anions and four equatorial lattice waters in the 1st-shell coordination sphere of Co^{2+}. The two remaining waters of hydration are 'free', but they reside near the apical chlorides and form hydrogen bonds with these anions [28]. Several 6-coordinate Co^{2+} complexes with multiple nitrogen-containing ligands have been prepared and characterized [29–31]. These coordination compounds support the concept that multiple amino ligands in poly(vinylamine) could displace lattice waters and occupy sites in the coordination sphere of Co^{2+}, which is a borderline acid [19,20].

1.4. Nickel d^8 complexes

Nickel(II) complexes are useful to induce synergistic T_g response in amorphous polymers with nitrogen-containing ligands in the sidegroup. The hexahydrates of nickel chloride and cobalt chloride adopt the same coordination number and ligand arrangement [32]. Nickel acetate tetrahydrate exhibits a pseudo-octahedral geometry in the solid state with four equatorial lattice waters and two apical monodentate acetate ligands [33,34]. In the most favorable situation, pseudo-octahedral Ni^{2+} forms metal–ligand σ-bonds with nitrogen lone pairs in two different macromolecular chains. Six-coordinate d^8 nickel complexes are strongly favored from an equilibrium viewpoint when good donor ligands are present [7]. Five-coordinate square pyramidal and trigonal bipyramidal complexes, and 4-coordinate tetrahedral and square planar complexes are also common [7]. This contribution proposes a previously unpublished mechanism by which nickel acetate tetrahydrate and nickel chloride hexahydrate enhance the glass transition temperature of poly(4-vinylpyridine) [2,8,15] and poly(L-histidine) [17], respectively.

2. Experimental considerations

2.1. Materials

Poly(vinylamine) (PVA) was supplied by Dr. Lloyd M. Robeson at Air Products and Chemicals, Inc. in Allentown, PA. It was synthesized from vinylformamide upon hydrolysis of the amide bond in the sidegroup of poly(vinylformamide). Linear PVA was provided in a free base aqueous solution (i.e. 32.5 wt% polymer, pH ≈ 10) with a weight-average molecular weight of 2.3×10^4 D, and a T_g of 57°C.

Table 1
Classification and characterization of polymers with attractive ligands in the main chain or the sidegroup

Polymer, acronym	Molecular weight (D)	T_g (°C)	HSAB class	pK_b (at 25°C)
Poly(vinylamine), PVA	2.3×10^4	57	Hard	3.34
Poly(4-vinylpyridine), P4VP	2×10^5	145	Borderline	8.75
Poly(L-histidine), PHIS	$1.5–5.0 \times 10^4$	169	–	8.0

Poly(4-vinylpyridine), P4VP, with a molecular weight of 2×10^5 D, was obtained from Scientific Polymer Products in Ontario, New York. Poly(L-histidine), with a molecular weight range of 1.5×10^4–5.0×10^4 D, was purchased from Sigma Chemical Company in St Louis, MO. Cobalt chloride hexahydryate, a reddish-pink powder, was purchased from Johnson Matthey Electronics in Ward Hill, MA. Nickel chloride hexahydrate (green powder), nickel acetate tetrahydrate (light green powder), and the dimer of dichlorotricarbonylruthenium(II) (yellow powder) were purchased from Aldrich Chemical Company in Milwaukee, WI.

2.2. Sample preparation methods

Poly(vinylamine)/Co^{2+} complexes were prepared in aqueous media at pH ≈ 9–10 by (i) mixing the polymer and metal-salt solutions, (ii) allowing the solvent to evaporate from a Petri dish in a fume hood at ambient temperature, and (iii) exposing the residual solids to further drying under vacuum at ambient temperature for at least 24 h, and an additional 24 h between 80 and 90°C. Nickel acetate tetrahydrate and P4VP were prepared in 3% (v/v) acetic acid. Cobalt chloride hexahydrate and P4VP were prepared from ethanol. Dichlorotricarbonylruthenium(II) and P4VP were prepared from methylene chloride under a nitrogen purge. Divalent transition metal complexes with poly(L-histidine) were prepared in aqueous media at a pH between 5 and 6. In each case, the total solids content was between 1 and 2% (w/v). Sample compositions indicate the mole fraction of d-block cations with respect to the polymeric repeat unit. For complexes with $[Ru(CO)_3Cl_2]_2$, sample composition indicates the mole fraction of Ru^{2+} metal centers, assuming that all of the dimers have been cleaved at low salt concentrations.

2.3. Differential scanning calorimetry

Thermal analysis was performed on a Perkin–Elmer DSC-7 interfaced to a TAC-7/DX thermal analysis controller and a personal computer. After quenching polymer–metal complexes from the molten state, T_g was measured at a rate of 20°C/min. during the 2nd or 3rd heating trace in the calorimeter, under a nitrogen purge. T_g measurements in these complexes exhibit thermoreversibility, due to reproducible thermal behavior in successive heating and cooling traces.

3. Energetic ligand field models for d-block complexes

3.1. The methodology of transition metal coordination

When low-molecular-weight d-block metal complexes coordinate to ligands in the sidegroup of a polymer and increase its glass transition temperature [2], predictions of this synergistic effect on T_g can be rationalized using the methodology discussed below. The overall objective of this study was to (i) estimate differences between electronic energies of a d^n configuration for macromolecule–metal complexes in the glassy and molten states, and (ii) correlate this electronic energy difference with the enhancement in the glass transition temperature. If one considers the increasingly exothermic enthalpy of formation of divalent hexa–aqua transition metal complexes [i.e. $M^{2+}(H_2O)_6$] as a function of the number of d-electrons from calcium (d^0) to zinc (d^{10}) [6,35], then the additional exothermic effect relative to linear trends from Ca^{2+} to Mn^{2+} and Mn^{2+} to Zn^{2+} correlates with the stabilization of metal d-electrons for octahedral complexes in the 1st row of the d-block with weak field electronic configurations. For trivalent metal cations in the 1st row of the d-block from scandium (d^0) to gallium (d^{10}), the increasingly exothermic enthalpy of formation for the following solid hexafluoro complexes [i.e. $K_3\{M^{3+}F_6\}^{3-}$] exhibits 'double-humped' behavior [35] as a function of the number of d-electrons, similar to that for hydration enthalpies. In this case, stabilization of metal d-electrons accounts for most, but not all, of the difference between actual data and smooth trend for these solid hexafluoro complexes. These empirical correlations between thermodynamic properties and d-electron energies of octahedral complexes provide support for correlating T_g enhancements in macromolecule–metal complexes with ligand-field-induced stabilization of metal d-electrons. Furthermore, this stabilization must be larger for complexes in the glassy state relative to the corresponding molten state complexes to realize metal-induced increases in the glass transition temperature with respect to T_g of the undiluted polymer [8,15].

3.2. Well-defined low-molecular-weight transition metal complexes

X-ray crystallography data from the research literature [22,23,26–28,32–34] reveal that all of the low-molecular-weight transition metal complexes analyzed in this study are pseudo-octahedral with a coordination number of six. In the

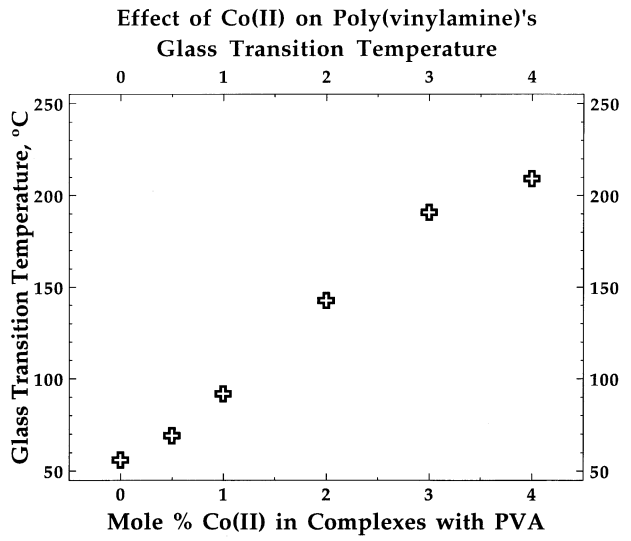

Fig. 1. Effect of cobalt chloride hexahydrate on the glass transition temperature of poly(vinylamine). Adopted from Refs. [9,16].

glassy state, all macromolecule–metal complexes are assumed to be six coordinate. However, in some cases, color changes might suggest that a geometric perturbation occurs. For example, the pink hexahydrate of cobalt chloride is 6-coordinate, whereas the blue anhydrous salt is 4-coordinate [26,28]. The hardness of each divalent transition metal cation (i.e. Ru^{2+}, Co^{2+} and Ni^{2+}) as a Lewis acid is classified as borderline.

3.3. Attractive polymeric ligands

The polymers discussed herein, which contain functional groups that coordinate to transition metal complexes, are summarized in Table 1. In addition to the hardness scale, 'reactive blending' is based on the fact that selected functional groups in the sidegroup of the polymer are stronger bases than the original weakly bound neutral ligands in the coordination sphere of the transition metal. Hence, these polymeric ligands will displace neutral ligands, like lattice waters or carbonyls. In most cases, weak-base neutral ligands are displaced by strong-base polymeric ligands that are also neutral. In less frequent situations, polymeric ligands cleave dimeric transition metal complexes, like dichlorotricarbonylruthenium (II), and coordinate to the vacant site after cleavage [22,23]. The hard and soft acid–base theory [19,20] is useful for selecting proper combinations of polymeric ligands and transition metal cations. There is an affinity between acids and bases with the same classification (i.e. hard acid/hard base, soft acid/soft base and borderline acid/borderline base). If there is a mismatch in hardness between the metal cation and a neutral ligand in the original low-molecular-weight complex, then this metal–ligand bond is the focal point for ligand exchange. Lattice waters are neutral hard bases, chloride anions are hard but weak [6] bases, and most of the late divalent metal cations in the 1st and 2nd rows of the d-block are borderline acids, but palladium (II) is soft [19].

3.4. Ligand exchange

Macromolecule–metal complexes described herein are based on ligand exchange [3], which represents a subset of generalized 'reactive blending' strategies to modify the thermophysical properties of polymers. This is illustrated schematically in Eq. (1) for divalent transition metal (M) chlorides with four weak-base waters of hydration in the 1st shell, some of which are displaced by strong-base polymeric ligands;

$$MCl_2(H_2O)_4 + x[\text{Polymer}] \leftrightarrow MCl_2[\text{Polymer}]_x(H_2O)_{4-x} + xH_2O \quad (1)$$

where $x \leq 4$. When weak bases are displaced by stronger bases, the metal–ligand σ-bonds which form are stronger than those that are dissociated.

3.5. Anionic ligands can be displaced to the 2nd shell

As illustrated by Eq. (1), weak basic neutral ligands with a different hardness classification than the metal center are most susceptible to displacement reactions. If $x > 4$ in Eq. (1), then all of the lattice waters and some of the weak base chloride anions are displaced by strong-base polymeric ligands;

$$MCl_2(H_2O)_4 + (4 + y)[\text{Polymer}] \leftrightarrow MCl_{2-y}[\text{Polymer}]_{4+y} + yCl^- + 4H_2O \quad (2)$$

where $y \leq 2$, and the displaced anionic ligands reside in the 2nd shell. For example, cobalt chloride hexahydrate forms complexes with poly(vinylamine) [9,16] when the lone pair on the amino nitrogen displaces all four waters of hydration in the 1st shell. It is also possible that amino nitrogens displace one or both of the chlorides to the 2nd shell [29–31]. Hence, cobalt (II) acts as a multifunctional bridge between several amino sidegroups. This is a reasonable structure which explains the unusually large increase in T_g for $CoCl_2(H_2O)_6$ complexes with poly(vinylamine) (i.e. ≈45°C/mol% Co^{2+}, up to 3 mol% Co^{2+}) [9,11,16], as illustrated in Fig. 1. Contrary to the results discussed below for complexes with poly(4-vinylpyridine and poly(L-histidine), which are much weaker bases than poly(vinylamine), Co^{2+} performs exceptionally well with poly(vinylamine) due to its ability to coordinate to several amino groups, as described generically by Eq. (2). This is not possible for dichlorotricarbonylruthenium(II) because it is increasingly difficult for amino sidegroups in poly(vinylamine) to displace more than one carbonyl ligand in the ruthenium complex after cleaving the dichloride bridge [22,23]. Hence, $CoCl_2(H_2O)_6$ is superior to $[RuCl_2(CO)_3]_2$ from the

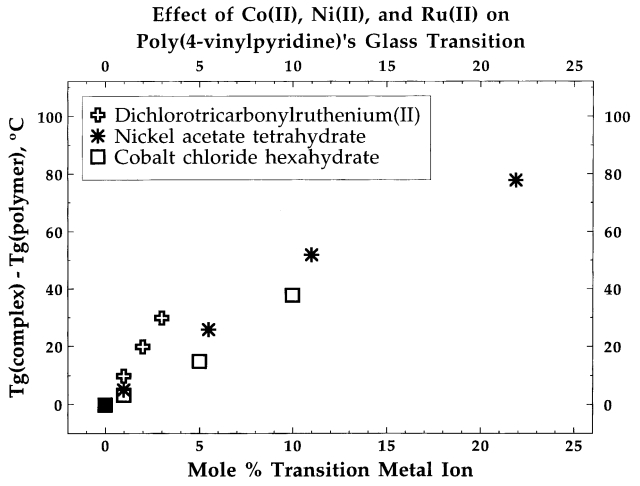

Fig. 2. Effect of cobalt chloride hexahydrate, nixckel acetate tetrahydrate, and dichlorotricarbonylruthenium(II) on the glass transition temperature of poly(4-vinylpyridine). Adopted from Refs. [2,8,15].

viewpoint of enhancing the glass transition temperature of poly(vinylamine) [11,16], based on a reduction in chain mobility via the number of NH_2 sidegroups that can occupy sites in the coordination sphere of Co^{2+} vs. Ru^{2+}, where the former cation contains weak-base lattice waters and the latter cation contains CO ligands.

3.6. Complexes with reduced symmetry above T_g

If T_g of the macromolecule–metal complex is higher than T_g of the undiluted polymer, then it is reasonable to consider that the glass transition occurs when sufficient thermal energy is provided to remove all but one of the polymeric ligands from the 1st shell coordination sphere of the transition metal [8,9,15]. Now, the transition metal complex represents a bulky coordination pendant group in the molten state. Furthermore, this complex which survives above T_g exhibits reduced symmetry and a decrease in coordination number because it is coordinatively unsaturated [3]. This is illustrated by Eq. (3) for divalent ruthenium complexes with two neutral carbonyls, two anionic chlorides, and two polymeric ligands in the 1st-shell coordination sphere;

$$RuCl_2(CO)_2[Polymer]_2 \leftrightarrow RuCl_2(CO)_2[Polymer] + Polymer \quad (3)$$

In the most favorable situation, the complex on the left side of Eq. (3) represents a 'coordination crosslink' in the glassy state, where ligands on two different polymer chains occupy sites in the 1st-shell of Ru^{2+}. There is infrared spectroscopic evidence [36] that this type of structure forms when pyridine ligands in the sidegroup of poly(4-vinylpyridine) cleave the dichloride bridge of the ruthenium dimer [i.e. $\{RuCl_2(CO)_3\}_3$]. The effect of Ru^{2+} on the glass transition temperature of poly(4-vinylpyridine) is illustrated in Fig. 2. The 5-coordinate complex on the right side of Eq. (3) represents a bulky 'coordination pendant group' in the molten state. When geometric perturbations occur, like the one illustrated in Eq. (3) which simulates structural modifications that are consistent with the onset of T_g, ligand field stabilization energies (LFSE) for metal d-electrons in the state of lower symmetry require more complex methods of analysis in comparison with LFSE calculations for pseudo-octahedral geometries. LFSE calculations for three possible 5-coordinate d^n complexes in the molten state are summarized below. All of these five-coordinate geometries are considered when distortions are allowed and the onset of T_g corresponds to the dissociation of one polymeric sidegroup from the coordination sphere of a pseudo-octahedral transition metal complex.

3.7. d-Orbital energies for five-coordinate complexes above T_g

Models are required to estimate the relative energies of the five d-orbitals in the molten state before ligand field stabilization energies can be calculated for 5-coordinate complexes. These orbital energies [37] are expressed in terms of the parameter D_q where $10D_q$ represents the corresponding octahedral ligand field splitting Δ_0. In terms of atomic parameters for octahedral complexes where six point charges, each one of magnitude $-ze$, are placed a distance L from the metal center with effective nuclear charge $+Ze$, D_q and C_p are defined as follows [37];

$$D_q = Zze^2\langle r^4\rangle/\{6L^5\} \quad (4)$$

$$7C_p/12D_q = L^2\langle r^2\rangle/\langle r^4\rangle \quad (5)$$

where $\langle r^n\rangle$ represents the average (i.e. expectation value) of r^n with respect to the radial part of the d-electron wavefunction, and r is the radius of the electron about the metal center. Hence, L corresponds to the metal–ligand bond distance, and $\langle r^n\rangle$ increases when the d-electron cloud experiences more delocalization due to the ligands via the nephelauxetic [35], or cloud expansion, effect.

3.7.1. Trigonal bipyramid d^n complexes with D_{3h} symmetry

Electronic energies relative to the five degenerate d-orbitals of the free metal ion have been compiled for trigonal bipyramid complexes [37]. This information is summarized in Table 2 for two different values (i.e. 1 or 2) of the atomic parameter defined in Eq. (5), where C_p/D_q is either 1.71 or 3.43 [37]. If each d-orbital is populated by a single electron, then the total electronic energy is exactly the same as that for the free metal ion, and there is no net stabilization due to the ligand field. Stabilization is prevalent when there is a larger population of electrons in lower energy orbitals. In a weak ligand field, electrons occupy vacant orbitals whenever possible, instead of pairing with opposite spin in lower energy orbitals. This usually results in less ligand field stabilization. In a strong ligand field, it is more probable that two electrons with opposite spin will be paired in lower energy

Table 2
Electronic energy calculations for 5-coordinate trigonal bipyramid complexes with D_{3h} symmetry

d-Orbital energies (Units of D_q) $7C_p/12D_q$	d_{xz}	d_{yz}	d_{xy}	$d_{x^2-y^2}$	d_{z2}
1	− 3.14	− 3.14	+ 0.035	+ 0.035	+ 6.21
2	− 2.72	− 2.72	− 0.815	− 0.815	+ 7.07

d-Electron configurations and ligand field stabilization energies No. of d-electrons	$7C_p/12D_q$	Ligand field Strength	d-Electron configuration	LFSE (D_q)
6	1	Weak	$\{xz\}^2\{yz\}^1\{xy\}^1\{x^2-y^2\}^1\{z^2\}^1$	3.14
6	2	Weak	$\{xz\}^2\{yz\}^1\{xy\}^1\{x^2-y^2\}^1\{z^2\}^1$	2.72
6	1	Strong	$\{xz\}^2\{yz\}^2\{xy\}^1\{x^2-y^2\}^1$	12.51
6	2	Strong	$\{xz\}^2\{yz\}^2\{xy\}^1\{x^2-y^2\}^1$	12.51
7	1	Weak	$\{xz\}^2\{yz\}^2\{xy\}^1\{x^2-y^2\}^1\{z^2\}^1$	6.28
7	2	Weak	$\{xz\}^2\{yz\}^2\{xy\}^1\{x^2-y^2\}^1\{z^2\}^1$	5.44
7	1	Strong	$\{xz\}^2\{yz\}^2\{xy\}^2\{x^2-y^2\}^1$	12.46
7	2	Strong	$\{xz\}^2\{yz\}^2\{xy\}^2\{x^2-y^2\}^1$	13.33
8	1	Weak	$\{xz\}^2\{yz\}^2\{xy\}^2\{x^2-y^2\}^1\{z^2\}^1$	6.25
8	2	Weak	$\{xz\}^2\{yz\}^2\{xy\}^2\{x^2-y^2\}^1\{z^2\}^1$	6.26
8	1	Strong	$\{xz\}^2\{yz\}^2\{xy\}^2\{x^2-y^2\}^2$	12.42
8	2	Strong	$\{xz\}^2\{yz\}^2\{xy\}^2\{x^2-y^2\}^2$	14.14

orbitals, instead of occupying vacant higher energy orbitals. In general, larger ligand field stabilization energies are possible in a strong ligand field. The z^2 orbital in trigonal bipyramid complexes with 6, 7 or 8 metal d-electrons remains vacant in a strong ligand field because the energy difference between d_{z^2} and $d_{x^2-y^2}$ is approximately 60–80% of the octahedral ligand field splitting. This methodology is employed to (i) determine the electronic configuration of d^6, d^7 and d^8 complexes in weak and strong fields, and (ii) calculate the energetic stabilization of metal d-electrons in terms of D_q, relative to the free metal ion. These calculations in Table 2 were performed for complexes with 6, 7 and 8 d-electrons in an effort to analyze the effects of Ru^{2+}, Co^{2+} and Ni^{2+} complexes on the glass transition temperature of poly(4-vinylpyridine) and poly(L-histidine), where pseudo-octahedral geometries with two polymeric ligands in the coordination sphere of a single metal center represent reasonable structures in the glassy state. The appropriate T_g enhancements are illustrated in Fig. 2 for poly(4-vinylpyridine) and Fig. 3 for poly(L-histidine). Once D_q is measured or predicted, the information in Table 2 is useful to estimate the energetic stabilization of metal d-electrons for coordinatively unsaturated trigonal bipyramid complexes in the molten state.

3.7.2. Square pyramid d^n complexes with C_{4v} symmetry

The methodology discussed in the previous section is repeated here for square pyramid complexes when all bond angles are 90°. Energies of the five d-orbitals [37] are summarized in Table 3, where an energy of zero is assigned to the degenerate orbitals of the free metal ion. The $x^2 - y^2$ d-orbital remains vacant for all complexes that contain eight electrons or less, when the ligand field is strong. For d^6 complexes with $7C_p/12D_q = 1$ in a strong ligand field, d_{z^2} is vacant because the energy difference between d_{z^2} and d_{xy} is more than 51% of the octahedral ligand field splitting. The calculations in Table 3 consider 5-coordinate complexes with either 6, 7 or 8 metal d-electrons. LFSE predictions in the far right column of this table are useful to analyze molten state complexes with reduced symmetry.

3.7.3. Pentagonal planar d^n complexes with D_{5h} symmetry

These 5-coordinate complexes exhibit d-orbital energies [37] that are summarized in Table 4. In the presence of a strong ligand field, d^6 complexes do not populate d_{xy} or $d_{x^2-y^2}$. There is no difference between weak field and strong field d^8 complexes because the two orbitals at highest energy are degenerate. LFSE calculations for these 5-coordinate

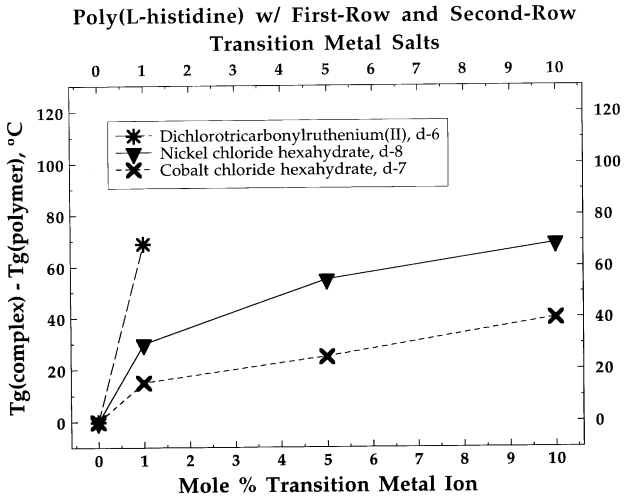

Fig. 3. Effect of $CoCl_2(H_2O)_6$, $NiCl_2(H_2O)_6$ and $\{RuCl_2(CO)_3\}_2$ on the glass transition temperature of poly(L-histidine). Adopted from Refs. [17,18].

Table 3
Electronic energy calculations for 5-coordinate square pyramid complexes with C_{4v} symmetry

d-Orbital energies (units of D_q) $7C_p/12D_q$	d_{xz}	d_{yz}	d_{xy}	d_{z^2}	$d_{x^2-y^2}$
1	− 3.715	− 3.715	− 2.57	+ 2.57	+ 7.43
2	− 4.57	− 4.57	− 0.86	+ 0.86	+ 9.14

d-Electron configurations and ligand field stabilization energies No. of d-electrons	$7C_p/12D_q$	Ligand field strength	d-Electron configuration	LFSE (D_q)
6	1	Weak	$\{xz\}^2\{yz\}^1\{xy\}^1\{z^2\}^1\{x^2-y^2\}^1$	3.72
6	2	Weak	$\{xz\}^2\{yz\}^1\{xy\}^1\{z^2\}^1\{x^2-y^2\}^1$	4.57
6	1	Strong	$\{xz\}^2\{yz\}^2\{xy\}^2$	20.00
6	2	Strong	$\{xz\}^2\{yz\}^2\{xy\}^1\{z^2\}^1$	18.28
7	1	Weak	$\{xz\}^2\{yz\}^2\{xy\}^1\{z^2\}^1\{x^2-y^2\}^1$	7.43
7	2	Weak	$\{xz\}^2\{yz\}^2\{xy\}^1\{z^2\}^1\{x^2-y^2\}^1$	9.14
7	1	Strong	$\{xz\}^2\{yz\}^2\{xy\}^2\{z^2\}^1$	17.43
7	2	Strong	$\{xz\}^2\{yz\}^2\{xy\}^2\{z^2\}^1$	19.14
8	1	Weak	$\{xz\}^2\{yz\}^2\{xy\}^2\{z^2\}^1\{x^2-y^2\}^1$	10.00
8	2	Weak	$\{xz\}^2\{yz\}^2\{xy\}^2\{z^2\}^1\{x^2-y^2\}^1$	10.00
8	1	Strong	$\{xz\}^2\{yz\}^2\{xy\}^2\{z^2\}^2$	14.86
8	2	Strong	$\{xz\}^2\{yz\}^2\{xy\}^2\{z^2\}^2$	18.28

complexes are summarized in the far right column of Table 4.

3.8. Summary of LFSE calculations for 5-coordinate d^n complexes

Ligand field stabilization energies for all possible 5-coordinate geometries of a d^n complex in either weak or strong fields are averaged with equal weighting factors. These results are summarized in Table 5. For d^6, d^7 and d^8 complexes, the dependence of LFSE on the number of d-electrons follows opposite trends for weak and strong ligand fields. All calculations are presented in units of D_q, defined in Eq. (4), where the corresponding octahedral ligand field splitting is given by $10D_q$. Parametric estimates of D_q are summarized in the following section for (i) pseudo-octahedral mixed ligand complexes with two polymeric ligands in the glassy state, and (ii) 5-coordinate mixed ligand complexes with one polymeric ligand above the glass transition temperature.

3.9. Jørgensen's group contribution method and parameters for octahedral ligand field splittings

Quantum chemical group contribution predictions which agree with the spectrochemical series are employed to estimate the octahedral ligand field splitting Δ_0 for six-coordinate complexes [35,37,38]. Jørgensen's predictive method contains a metal-based *g*-parameter and a ligand-based *f*-parameter when all six monodentate ligands in the 1st-shell coordinate sphere are identical. The metal-based *g*-parameter provides the strongest influence on Δ_0. Since one

Table 4
Electronic energy calculations for 5-coordinate pentagonal planar complexes with D_{5h} symmetry

d-Orbital energies (units of D_q) $7C_p/12D_q$	d_{xz}	d_{yz}	d_{z^2}	d_{xy}	$d_{x^2-y^2}$
1	− 4.29	− 4.29	− 1.07	+ 4.825	+ 4.825
2	− 6.42	− 6.42	− 5.35	+ 9.10	+ 9.10

d-Electron configurations and ligand field stabilization energies No. of d-electrons	$7C_p/12D_q$	Ligand field strength	d-Electron configuration	LFSE (D_q)
6	1	Weak	$\{xz\}^2\{yz\}^1\{z^2\}^1\{xy\}^1\{x^2-y^2\}^1$	4.29
6	2	Weak	$\{xz\}^2\{yz\}^1\{z^2\}^1\{xy\}^1\{x^2-y^2\}^1$	6.42
6	1	Strong	$\{xz\}^2\{yz\}^2\{z^2\}^2$	19.30
6	2	Strong	$\{xz\}^2\{yz\}^2\{z^2\}^2$	36.38
7	1	Weak	$\{xz\}^2\{yz\}^2\{z^2\}^1\{xy\}^1\{x^2-y^2\}^1$	8.58
7	2	Weak	$\{xz\}^2\{yz\}^2\{z^2\}^1\{xy\}^1\{x^2-y^2\}^1$	12.84
7	1	Strong	$\{xz\}^2\{yz\}^2\{z^2\}^2\{xy\}^1$	14.48
7	2	Strong	$\{xz\}^2\{yz\}^2\{z^2\}^2\{xy\}^1$	27.28
8	1	Weak,strong	$\{xz\}^2\{yz\}^2\{z^2\}^2\{xy\}^1\{x^2-y^2\}^1$	9.65
8	2	Weak, strong	$\{xz\}^2\{yz\}^2\{z^2\}^2\{xy\}^1\{x^2-y^2\}^1$	18.19

Table 5
Averaged ligand field stabilization energies for 5-coordinate d^n complexes

No. of d-electrons	Ligand field strength	LFSE (D_q)
d^6	Weak	4.14
d^6	Strong	19.83
d^7	Weak	8.29
d^7	Strong	17.35
d^8	Weak	10.06
d^8	Strong	14.59

wavenumber (i.e. 1 cm^{-1}) corresponds to 11.963 J/mol, the following expression is useful to estimate Δ_0 with units of kJ/mol;

$$\Delta_0 = 10D_q = 11.963\{f\}\{g\} \quad (6)$$

Table 6 contains Jørgensen's parameters [35,37,38] for the divalent metal cations of interest in this study, and all of the appropriate anionic and neutral ligands in the original low-molecular-weight complexes, as well as those in the sidegroups of the polymers. The *f*-parameter for CO (i.e. ≈5–7) was calculated from Eq. (6) using experimental data for $\{Mn(CO)_6\}^{+1}$ (i.e. $\Delta_0 = 41650\ cm^{-1}$) [39,40]. The *g*-parameters for Mn^{2+}, Mn^{3+} and Mn^{4+} are 8.5, 21 and 23, respectively [35,38], which reveal that Δ_0 is smaller when the metal is in a lower oxidation state. This is consistent with the fact that D_q is reduced, via Eq. (4), when the effective nuclear charge experienced by the ligands (i.e. +Ze) is smaller. Hence, the *g*-parameter for Mn^{+1} is less than 8.5. The relatively large *f*-parameter for carbonyl ligands is consistent with the fact that CO is the strongest π-acceptor in the spectrochemical series [6]. The *f*-parameter for imidazole was determined from an empirical correlation between Brønsted ionization equilibrium constants [6] (i.e. pK_b) and Jørgensen's *f*-parameters [35,37,38] for three anionic ligands (i.e. Br^-, Cl^-, and CN^-) and two neutral ligands (i.e. H_2O and C_5H_5N). *f*-Parameters and pK_bs for these five ligands are included in Table 6. The following 3rd-order polynomial was used to (i) match these five data pairs for *f* vs. pK_b with a correlation coefficient better than 0.999 and (ii) estimate the Jørgensen *f*-parameter for six monodentate imidazole ligands, which is within the range of the data set;

$$f = 2.61 - 2.51\times10^{-1}\{pK_b\} + 1.31\times10^{-2}\{pK_b\}^2 - 2.52\times10^{-4}\{pK_b\}^3 \quad (7)$$

Since the Brønsted ionization equilibrium constant for the imidazole ring [41] in histidine is $pK_b = 8.0$, the Jørgensen *f*-parameter for imidazole is estimated to be 1.32, as indicated in Table 6. The 'rule of average environments' [35,38] is invoked to calculate pseudo-octahedral ligand field splittings for mixed ligand complexes that are 6-coordinate below T_g and 5-coordinate above T_g. In other words, the concept of the magnitude of a cubic ligand field is appropriate for complexes that are only approximately cubic in symmetry [38]. The averaging is performed as follows. For 6-coordinate complexes with three different types of ligands, denoted by $M^{2+}(L_1)_2(L_2)_2(L_3)_2$, the pseudo-octahedral ligand field splitting in kJ/mol is estimated by;

$$\{\Delta_0\}_{6\text{-coordinate}} = \{10D_q\}_{6\text{-coordinate}} = 11.963g(M^{2+})\{f(L_1) + f(L_2) + f(L_3)\}/3 \quad (8)$$

For 5-coordinate complexes with three different types of ligands, denoted $M^{2+}(L_1)_2(L_2)_2(L_3)_2$, the corresponding 'pseudo-octahedral' ligand field splitting in kJ/mol is estimated by;

$$\{\Delta_0\}_{5\text{-coordinate}} = \{10D_q\}_{5\text{-coordinate}} = 11.963g(M^{2+})\{2/5)f(L_1) + (2/5) + f(L_2) + (1/5)f(L_3)\} \quad (9)$$

where anionic, neutral and polymeric ligands are denoted by L_1, L_2, and L_3, respectively. This procedure is employed to estimate Δ_0 for all complexes in the following scheme, based on Eq. (3), which represents the onset of T_g in macromoledule–metal complexes with enhanced glass transition temperatures relative to the undiluted polymers;

$$M^{2+}(L_1)_2(L_2)_2(L_3)_2 \leftrightarrow M^{2+}(L_1)_2(L_2)_2L_3 + L_3 \quad (10)$$

where M^{2+} is either Ru^{2+}, Co^{2+} or Ni^{2+}; L_1 is either Cl^-or CH_3COO^-; L_2 is either H_2O or CO; and L_3 is the nitrogen lone pair in the sidegroup of either poly(4-vinylpyridine) or poly(L-histidine). Reactive blending based on Eq. (1) with $x = 2$ is responsible for the 6-coordinate complex below T_g on the left side of Eq. (10). Pseudo-octahedral ligand field splittings Δ_0 are computed in Table 7 for complexes on the left and right sides of Eq. (10) using Eqs. (8) and (9), respectively, for systems whose T_g behavior is presented in Figs. 2 and 3. An average *f*-parameter of 6.0 was employed for CO ligands.

Table 6
Jørgensen's *g*-parameters for metal cations and *f*-parameters for anionic and neutral ligands. pK_bs are included for ligand functional groups that were used to construct the empirical correlation given by Eq. (7)

Metal cations	*g*-Parameter	Ligands	pK_b	*f*-Parameter
Ni^{2+}	8.8	6 Br^-	23	0.74
Co^{2+}	9.2	6 Cl^-	21	0.79
Ru^{2+}	20.0	6 CH_3COO^-		0.95
		6 H_2O	14	1.00
		6C_5H_5N[a]	8.75	1.24
		6[PHIS][b]	8.0	1.32
		6 CN^-	4.69	1.7
		6 CO		5–7

[a] C_5H_5N represents a pyridine ring in the sidegroup of poly(4-vinylpyridine).
[b] [PHIS] is an acronym for the imidazole ring in the histidine sidegroup of poly(L-histidine).

Table 7
Ligand field splittings and LFSEs for macromolecule–metal complexes above and below the glass transition temperature

	$10D_q$ (kJ/mol)	Ligand field strength	LFSE (kJ/mol)
d^6 Complexes			
$RuCl_2(CO)_2[P4VP]_2$	640	Weak	$4D_q = 256$
		Strong	$24D_q = 1536$[a]
$RuCl_2(CO)_2[P4VP]$	709	Weak	$4.14D_q = 294$
		Strong	$19.83D_q = 1406$[a]
$RuCl_2(CO)_2[PHIS]_2$	647	Weak	$4D_q = 259$
		Strong	$24D_q = 1553$[a]
$RuCl_2(CO)_2[PHIS]$	713	Weak	$4.14D_q = 295$
		Strong	$19.83D_q = 1414$[a]
d^7 Complexes			
$CoCl_2(H_2O)_2[P4VP]_2$	111	Weak	$8D_q = 88.9$[a]
		Strong	$18D_q = 200$
$CoCl_2(H_2O)_2[P4VP]$	106	Weak	$8.29D_q = 88.0$[a]
		Strong	$17.35D_q = 184$
$CoCl_2(H_2O)_2[PHIS]_2$	114	Weak	$8D_q = 91.3$[a]
		Strong	$18D_q = 205$
$CoCl_2(H_2O)_2[P4VP]$	108	Weak	$8.29D_q = 89.4$[a]
		Strong	$17.35D_q = 187$
d^8 Complexes			
$Ni(CH_3COO)_2(H_2O)_2[P4VP]_2$	112	Weak	$12D_q = 134$[a]
		Strong	$12D_q = 134$
$Ni(CH_3COO)_2(H_2O)_2[P4VP]$	108	Weak	$10.06D_q = 109$[a]
		Strong	$14.59D_q = 158$
$NiCl_2(H_2O)_2[PHIS]_2$	109	Weak	$12D_q = 131$[a]
		Strong	$12D_q = 131$
$NiCl_2(H_2O)_2[PHIS]$	103	Weak	$10.06D_q = 104$[a]
		Strong	$14.59D_q = 150$

[a] Most probable LFSE for d^n complexes based on a consideration of Δ_0 and interelectronic repulsion.

3.10. Consideration of interelectronic repulsion and Δ_0 when there is ambiguity in the d-electron configuration for complexes with pseudo-octahedral symmetry

There is ambiguity in the electronic configuration for d^6 and d^7 octahedral (i.e. O_h) complexes when the following two possibilities exist; (1) two electrons with opposite spin occupy a lower energy orbital in a strong ligand field, or (2) higher energy orbitals contain unpaired electrons in a weak ligand field. The most energetically favorable configuration is determined by estimating the Racah interelectronic repulsion parameter B;

$$B = B_0(1 - hk) \tag{11}$$

for 6-coordinate complexes with O_h symmetry if B_0 is known for the free metal cation [35,38]. The parameters h and k are characteristic of the ligand and metal, respectively. As a consequence of the delocalization of metal d-electrons over the ligands, interelectronic repulsion is weaker [6] and the Racah B parameter is reduced in magnitude relative to B_0 for the free metal cation. Table 8 summarizes information about d-orbital energies, B_0 for Ru^{2+}, Co^{2+} and Ni^{2+}, crossover energies for weak and strong ligand fields in terms of $\{\Delta_0/B\}_{critical}$, weak field and strong field electronic configurations, and the corresponding LFSEs for d^6, d^7 and d^8 6-coordinate complexes. For Ru^{2+} in the 2nd-row of the d-block, the large g-parameter (i.e. 20), the extremely large f-parameter for CO, and the small value of B_0 (620 cm^{-1}) [35,38] suggest that strong field electronic configurations are most probable for these heavy metal d^6 complexes because Δ_0/B is invariably greater than the weak-field/strong-field crossover [6,35] at 18–20. Hence, d_{xy}, d_{yz} and d_{xz} are doubly populated, d_{z^2} and $d_{x^2-y^2}$ are vacant, and LFSE is $24D_q$. For Co^{2+} in the 1st-row of the d-block, a much smaller g-parameter (i.e. 9.2) and a very large value of B_0 (i.e. 1120 cm^{-1}) [38], with no carbonyl ligands, argue in favor of a weak field electronic configuration with Δ_0/B less than the crossover [6,35] at 21–23. Now, the higher energy d-orbitals (i.e. d_{z^2} and $d_{x^2-y^2}$) contain one electron each, and LFSE is $8D_q$. There is no ambiguity in electronic configuration for d^8 Ni^{2+} complexes with octahedral symmetry. However, ligand field strength, or Δ_0/B, influences the electronic configuration for 5-coordinate d^8 complexes. Since B_0 and Jørgensen's g-parameter for Ni^{2+} are similar to those for Co^{2+}, and no carbonyl ligands occupy sites in the 1st-shell of Ni^{2+} for the complexes of interest, it is reasonable to adopt weak field electronic configurations for $Ni(CH_3COO)_2(H_2O)_2$[P4VP] and $NiCl_2(H_2O)_2$[PHIS] in the molten state.

Table 8
Racah interelectronic repulsion parameters for free metal cations, weak/strong field crossover energies, d-electron configurations and LFSEs for pseudo-octahedral d^n complexes (note: d_{xy}, d_{yz} and d_{xz} (denoted by t_{2g}) are degenerate at $-4D_q$; d_{z^2} and $d_{x^2-y^2}$ (denoted by e_g) are degenerate at $+6D_q$)

	B_0 (cm^{-1})	$\{\Delta_0/B\}$	d-Electron configuration	LFSE (D_q)
d^6 Complexes				
Ru^{2+}	620	<18–20	$\{t_{2g}\}^4\{e_g\}^2$	4
		>18–20	$\{t_{2g}\}^6$	24
d^7 Complexes				
Co^{2+}	1120	<21–22	$\{t_{2g}\}^5\{e_g\}^2$	8
		>21–22	$\{t_{2g}\}^6\{e_g\}^1$	18
d^8 Complexes				
Ni^{2+}	1080	–	$\{t_{2g}\}^6\{e_g\}^2$	12

3.11. Correlation between T_g enhancement and the difference between ligand field stabilization energies in the glassy and molten states

Ligand field stabilization energies are calculated in Table 7 for macromolecule–metal complexes on the left and right sides of Eq. (10) for both weak and strong ligand fields. Based on consideration of interelectronic repulsion in the previous section, superscripts in the far right column of Table 7 identify the most probable LFSEs for 5- and 6-coordinate complexes of Ru^{2+}(i.e, strong field), Co^{2+} (i.e. weak field) and Ni^{2+} (weak field). When the appropriate ligand field strength is considered in Table 7, LFSEs are larger for glassy 6-coordinate complexes than they are for 5-coordinate complexes above T_g. More stabilization of metal d-electrons due to geometry and the surrounding ligands in the glassy state is consistent with the fact that these complexes exhibit thermochemical synergy with respect to T_g, upon removal of one polymeric ligand from the 1st-shell. This is analogous to the fact that larger LFSEs for $\{M(H_2O)_6\}^{2+}$ yield more exothermic hydration enthalpies relative to linear trends from Ca^{2+} to Mn^{2+} to Zn^{2+} for divalent hexa–aqua metal complexes from the 1st-row of the d-block [6,35]. Furthermore, when one lattice water is removed from these hexa–aqua complexes, the log of the kinetic rate constant for this process, or the free energy of activation from the 6-coordinate complex to the transition state, is correlated [37] empirically with the difference between LFSEs (i.e. units of D_q) of octahedral ML_6 and square pyramidal ML_5. In this research contribution, D_q is estimated for 5- and 6-coordinate mixed-ligand complexes above and below T_g. Then, the difference between LFSEs (i.e. units of kJ/mol) in the glassy and molten states is correlated with the increase in T_g for poly(4-vinylpyridine) and poly(L-histidine) complexes with Ru^{2+}, Co^{2+} and Ni^{2+}, at 1 mol% metal cation. These results are presented in Fig. 4. The reduction in chain mobility and the increase in T_g is more pronounced when the first trace of metal cation is present. There is further enhancement of T_g at higher concentrations of metal cations, but the 'relative' increase

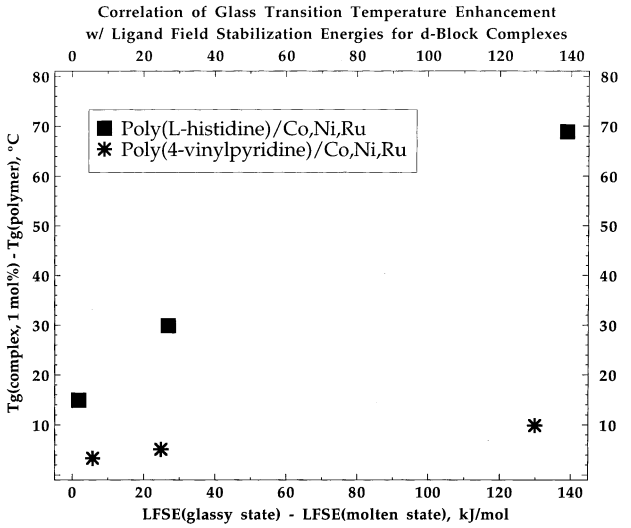

Fig. 4. Correlation between T_g enhancement at 1 mol% metal cation and ligand field stabilization energy differences below and above T_g for Ru^{2+}, Co^{2+} and Ni^{2+} complexes with poly(4-vinylpyridine) and poly(L-histidine).

in T_g is not as significant as the initial effect. Most T_g-composition behavior, experimental or theoretical, is nonlinear. Ligand field analysis is correlated with the initial slope of T_g vs. composition, in the range from 0 to 1 mol% metal cation. Without adjustable parameters which might account for differences in complexation efficiency between pyridine and imidazole, it is not possible to generate a universal correlation for T_g enhancement, based on the six complexes that were analyzed in this study. Nevertheless, a priori calculations of this nature, together with a reasonable model like Eq. (10) for the onset of T_g, are useful to identify macromolecule–metal complexes which exhibit thermochemical synergy.

3.12. Tetrahedral Co^{2+} complexes below T_g and 3-coordinate complex in the molten state

An alternate viewpoint of macromolecule–metal complexes with Co^{2+} is presented, when two ligands in the sidegroup of the polymer occupy sites in the 1st-shell coordination sphere of the metal center below T_g. As mentioned above, $CoCl_2(H_2O)_6$ is pink and the anhydrous salt is blue [26,28]. Cobalt chloride adopts a tetrahedral geometry in ethanol with a characteristic blue color [28]. X-ray diffraction data on dark blue crystals of dichlorobis(4-vinylpyridine)cobalt(II) suggest that the structure of this four-coordinate pseudo-tetrahedral complex contains two 4-vinylpyridine ligands and no waters of hydration [42–44]. These studies are significant because they demonstrate that the borderline acid Co^{2+} sheds its four hard-base lattice waters in favor of two borderline-base [19] pyridine ligands. Tetrahedral symmetry of the metal center is a common occurrence for d^7 Co^{2+} complexes [7]. If geometric perturbations occur during preparation of complexes with poly(4-vinylpyridine) in ethanol, then octahedral

Table 9
Electronic energy calculations for 3-coordinate (i.e. C_{3v} and D_{3h}) and 4-coordinate (i.e. T_d) d^7 Co^{2+} complexes which correspond to Eq. (12)

d-Orbital energies (D_q) for facial trivacant complexes with C_{3v} symmetry (all bond angles are 90°)

$7C_p/12D_q$	d_{xz}	d_{yz}	d_{xy}	$d_{x^2-y^2}$	d_{z^2}
1,2	− 2.00	− 2.00	− 2.00	+ 3.00	+ 3.00

d-Orbital energies (D_q) for trigonal planar complexes with D_{3h} symmetry (all bond angles are 120°)

$7C_p/12D_q$	d_{xz}	d_{yz}	d_{z^2}	d_{xy}	$d_{x^2-y^2}$
1	− 2.57	− 2.57	− 0.65	+ 2.895	+ 2.895
2	− 3.85	− 3.85	− 3.21	+ 5.46	+ 5.46

d-Orbital energies (D_q) for tetrahedral complexes with T_d symmetry

$7C_p/12D_q$	$d_{x^2-y^2}$	d_{z^2}	d_{xy}	d_{yz}	d_{xz}
1,2	− 2.67	− 2.67	+ 1.78	+ 1.78	+ 1.78

Ligand field stabilization energies for 3- and 4-coordinate d^7 complexes

Symmetry	$7C_p/12D_q$	Ligand field strength	d-Electron configuration	LFSE(D_q)
C_{3v}	1,2	Weak	$\{xz\}^2\{yz\}^2\{xy\}^1\{x^2-y^2\}^1\{z^2\}^1$	4.00
D_{3h}	1	Weak	$\{xz\}^2\{yz\}^2\{z^2\}^1\{xy\}^1\{x^2-y^2\}^1$	5.14
D_{3h}	2	Weak	$\{xz\}^2\{yz\}^2\{z^2\}^1\{xy\}^1\{x^2-y^2\}^1$	7.69
		Average LFSE for 3-coordinate complexes		5.21
T_d	1,2	Weak	$\{x^2-y^2\}^2\{z^2\}^2\{xy\}^1\{yz\}^2\{xz\}^1$	5.34

d^7 Complexes	State	$10D_q$ (kJ/mol)	LFSE (kJ/mol)
$CoCl_2[P4VP]_2$	Glass	111.7	$5.34D_q = 59.7$
$CoCl_2[P4VP]$	Molten	103.5	$5.21D_q = 53.9$
$CoCl_2[PHIS]_2$	Glass	116.1	$5.34D_q = 62.0$
$CoCl_2[PHIS]$	Molten	106.4	$5.21D_q = 55.4$

$CoCl_2(H_2O)_6$ might revert to tetrahedral coordination with two pyridine ligands and two anionic chloride ligands. If this 4-coordinate structure persists in the glassy state, then the onset of T_g might occur when one pyridine ligand in the sidegroup of the polymer is removed from the coordination sphere of Co^{2+} due to the addition of thermal energy. Now, the coordinatively unsaturated [3] molten state complex above T_g is 3-coordinate, and the possibilities range from facial trivacant (i.e. nonplanar), where all bond angles are 90°, to trigonal planar, where all bond angles are 120°. The following scheme represents a model for the glass transition process in Co^{2+} complexes with poly(4-vinylpyridine) that have been prepared from ethanol;

$$CoCl_2[P4VP]_2 \leftrightarrow CoCl_2[P4VP] + P4VP \quad (12)$$

Stabilization energies for metal d-electrons above and below T_g, based on Eq. (12) are presented in Table 9. Weak field electronic configurations are favored for 4- and 3-coordinate d^7 metal complexes from the 1st-row of the d-block, with no carbonyl ligands. One predicts that LFSE for 4-coordinate tetrahedral Co^{2+} complexes with poly(4-vinylpyridine) below T_g is larger than LFSE for the corresponding 3-coordinate complex in the molten state by 5.8 kJ/mol. Since these complexes were prepared in ethanol, the horizontal coordinate [i.e. Δ(LFSE)] of the empirical correlation for P4VP/Co^{2+} complexes in Fig. 4 is changed from 0.9 kJ/mol (Table 7) to 5.8 kJ/mol (Table 9). Previous analyses [15] of P4VP/Co^{2+} complexes that were assumed to be pseudo-tetrahedral above and below T_g yield LFSEs which are 3.7 kJ/mol larger in the glassy state relative to the molten state. Predictions for Co^{2+} complexes with poly(L-histidine), based on Eq. (12), reveal that LFSE in the glassy state is 6.6 kJ/mol larger than that in the molten state. However, these complexes were prepared in aqueous solution and lattice waters should be retained in the glassy state structure, represented schematically on the left side of Eq. (10). In this case, pseudo-octahedral glassy complexes revert to 5-coordinate complexes via the onset of T_g, so Δ(LFSE) of 1.9 kJ/mol from Table 7 is employed on the horizontal axis of Fig. 4 for poly(L-histidine) Co^{2+} instead of 6.6 kJ/mol calculated in Table 9.

4. Conclusions

Stabilization of metal d-electrons has been employed previously to explain thermodynamic [6,35] and kinetic [37] data for 6-coordinate hexa–aqua divalent transition metal complexes from the 1st-row of the d-block. Kinetic data in Ref. [37] were analyzed for a 5-coordinate square pyramidal complex in the transition state that was not allowed to distort. The methodology employed herein allows for geometric distortions in the molten state to model the glass transition process in macromolecule–metal complexes with enhanced T_gs. By focusing on weakly basic ligands with a different hardness classification than the metal center, ligand exchange in the 1st-shell coordination sphere of d-block cations was invoked to couple two different chains via coordination crosslinks. For complexes based on dichlorotricarbonylruthenium (II) at low metal

cation concentrations, group theory analysis of previous infrared data [36] yields a glassy state structure where two sidegroups from the polymer occupy sites in the 1st-shell of Ru^{2+}. Dissociation of one of these metal–polymer σ-bonds at high temperature produces a 5-coordinate complex with reduced symmetry in the molten state. Ligand field stabilization energy differences between 6-coordinate glassy complexes and 5-coordinate molten complexes have been correlated with the enhancement in T_g for Ru^{2+}, Co^{2+} and Ni^{2+} complexes with poly(L-histidine). For similar complexes with poly(4-vinylpyridine), Ru^{2+} and Ni^{2+} are considered to be pseudo-octahedral below T_g and 5-coordinate above T_g, but the corresponding Co^{2+} complexes prepared from ethanol are considered to be pseudo-tetrahedral below T_g and 3-coordinate above T_g. At 1 mol% of the d-block metal cations, there is much more enhancement in the glass transition of poly(L-histidine), relative to that for poly(4-vinylpyridine). Adjustable parameters were not introduced in the development of this correlation between $T_{g,complex}-T_{g,polymer}$ and the difference between ligand field stabilization energies below and above T_g. The model predicts thermochemical synergy for six different macromolecule–metal complexes. However, universality of the correlation has not been demonstrated for these six complexes, even though the basicity of the important functional group in the polymer's sidechain influences predictions of ligand field stabilization energies via Jørgensen's quantum chemical group contribution method.

Acknowledgements

The research described herein is supported by the National Science Foundation's Division of Materials Research, Polymers Program, through grant DMR-9902657.

References

[1] Kelley FN, Bueche F. J Polym Sci 1961;50:549.
[2] Belfiore LA, McCurdie MP. J Polym Sci Polym Phys Ed 1995;33:105.
[3] Hegedus LS. Transition metals in the synthesis of complex organic molecules. 2nd ed, vol. 4. Sausalito, CA: University Science Books, 1999. p. 13–5.
[4] Fujita H, Kishimoto A. J Polym Sci 1958;28:547.
[5] Fujita H, Kishimoto A. J Chem Phys 1961;34(2):393.
[6] Shriver DF, Atkins PW, Langford CH. Inorganic chemistry. New York: Freeman, 1990. p. 150, 206–211, 214, 445, 504–6, 683.
[7] Cotton FA, Wilkinson G. Advanced inorganic chemistry: a comprehensive text. 3rd ed. New York: Wiley–Interscience, 1972. Chapter 25, p. 875, 890–7.
[8] Belfiore LA, Graham HRG, Ueda E. Macromolecules 1992;25:2935.
[9] Belfiore LA, Indra EM, Das PK. Macromol Symp Polym–Solvent Complexes 1997;114:35.
[10] Das PK, Ruzmaikina IY, Belfiore LA. J Polym Sci Polym Phys Ed 2000;38:1931.
[11] Belfiore LA, Ruzmaikina IY, Das PK. Thermophysical property modifications in functional polymers via lanthanide trichloride hydrates. Polym Engng Sci 2001;41(7):1196.
[12] Bossé F, Das PK, Belfore LA. In: Hybrid organic inorganic composites, Mark JE, Lee CYC, Bianconi PA, editors. ACS symposium series 585, vol. 585. Washington, DC: American Chemical Society, 1995. p. 192.
[13] Bossé F, Das PK, Belfiore LA. Polym Gels Networks 1997;5(5):387.
[14] Tanaka T, Wang C, King K. Faraday Discuss 1995;101:201.
[15] Belfiore LA, McCurdie MP, Ueda E. Macromolecules 1993;26:6908.
[16] Belfiore LA, Indra EM. J Polym Sci Polym Phys Ed 552;38(4):2000.
[17] McCurdie MP, Belfiore LA. J Polym Sci Polym Phys Ed 1999; 37(4):301.
[18] McCurdie MP. PhD thesis, Colorado State University, 1997.
[19] Pearson RG. In: Scott A, editor. Survey of progress in chemistry, vol. 6. New York: Academic, 1969. p. 12–3, Chapter 1.
[20] Pearson RG, editor. Hard and soft acids and bases, Benchmark papers in inorganic chemistry. Stroudsburg, PA: Dowden, Hutchinson and Ross, Inc, 1973.
[21] Merlino S, Montagnoli G. Atti Soc Tosc Sci Nat 1970;76:335.
[22] Stephenson TA, Wilkinson G. J Inorganic Nuclear Chem 1966; 28:945.
[23] Benedetti E, Braca G, Sbrana G, Salvetti F, Grassi B. J Organomet Chem 1972;37:361.
[24] Bruce MI, Stone FGA. J Chem Soc 1967;A:1238.
[25] Cleare MJ, Griffith QP. J Chem Soc 1969;A:372.
[26] Young RS, editor. Cobalt: its chemistry, metallurgy and uses. New York: Reinhold, 1960. p. 76.
[27] Mizuno J, Ukei K, Sugawara T. J Phys Soc Jpn 1959;14:383.
[28] Nicholls D. In: Bailar JC, Emeléus HJ, Nyholm R, Trotman-Dickenson AF, editors. Cobalt, Comprehensive inorganic chemistry, vol. 3. Oxford: Pergamon, 1973.
[29] Pomogailo AD. In: Ciardelli F, Tsuchida E, Wöhrle D, editors. Macromolecule–metal complexes. Berlin: Springer, 1996. p. 52.
[30] House DA. In: Wllkinson G, Gillard RD, McCleverty JA, editors. Ammonia and amines, Comprehensive coordination chemistry: synthesis, reactions, properties and applications of coordination compounds, vol. 2. Oxford: Pergamon, 1987. p. 23–43, Chapter 13.1.
[31] Constable EC. Metals and ligand reactivity. New York: Ellis Horwood, 1990. p. 115.
[32] Wells AF. Structural inorganic chemistry. 5th ed. New York: Oxford University Press, 1984. p. 674–5.
[33] VanNiekerk JN, Schoening FRL. Acta Crystallogr 1953;6:609.
[34] Downie TC, Harrison W, Raper ES, Hepworth MA. Acta Crystallogr 1971;B27:706.
[35] Figgis BN, Hitchman MA. Ligand field theory and its applications. New York: Wiley–VCH, 2000. p. 18, 105, 139, 140, 167–71, 194–5, 218–21.
[36] McCurdie MP, Belfiore LA. Polymer 1999;40(11):2889.
[37] Burdett JK. Molecular shapes: theoretical models of inorganic stereochemistry. New York: Wiley–Interscience, 1980 p. 124–33, 138, 139, 167–9, 189.
[38] Figgis BN. An introduction to ligand fields. New York: Wiley–Interscience, 1966. p. 17, 52, 236–7, 244.
[39] Pruchnik FP. Organometallic Chemistry of the Transition Elements. New York: Plenum, 1990, translated by Duraj SA. p. 45.
[40] Beach NA, Gray HB. J Am Chem Soc 1968;90:5713.
[41] Bohinski RC. Modern concepts in biochemistry. 4th ed. Boston: Allyn and Bacon, 1983. p. 61.
[42] Admiraal LJ, Gafner G. The crystal and molecular structure of dichlorobis(4-vinylpyridine)cobalt(II). Chem Commun 1968:1221.
[43] Agnew NH, Larkworthy LF. Cobalt (II) complexes of 2-and 4-vinylpyridines. J Chem Soc 1965:4669.
[44] Gill NS, Hyholm RS, Barclay GA, Christie TI, Pauling PJ. J Inorganic Nuclear Chem 1961;18:88.